Off-axis electron cyclotron heating and the sandpile paradigm for transport in tokamak plasmas

T. K. March, S. C. Chapman, R. O. Dendy, and J. A. Merrifield

Off-axis electron cyclotron heating and the sandpile paradigm for transport in tokamak plasmas

T. K. March and S. C. Chapman
Space and Astrophysics Group, Department of Physics, Warwick University, Coventry CV4 7AL, United Kingdom

R. O. Dendy
EURATOM/UKAEA Fusion Association, Culham Science Centre, Abingdon, Oxfordshire OX14 3DB, United Kingdom
and Space and Astrophysics Group, Department of Physics, Warwick University, Coventry CV4 7AL, United Kingdom

J. A. Merrifield
Space and Astrophysics Group, Department of Physics, Warwick University, Coventry CV4 7AL, United Kingdom

Previous observations that suggest a substantial role for nondiffusive energy transport in tokamaks subjected to off-axis electron cyclotron heating (ECH) are compared to the output from a sandpile model. The observations considered include local and global aspects of temperature profile evolution in the DIII-D [for example, C. C. Petty and T. C. Luce, Nucl. Fusion **34**, 121 (1994)] and RTP (Rijnhuizen Tokamak Project) [for example, M. R. de Baar, M. N. A. Beurskens, G. M. D. Hogeweij, and N. J. Lopes Cardozo, Phys. Plasmas **6**, 4645 (1999)] tokamaks. The sandpile model employed is an extension, to incorporate noncentral fueling, of one used previously to address tokamak physics issues [S. C. Chapman, R. O. Dendy, and B. Hnat, Phys. Rev. Lett. **86**, 2814 (2001)]. It is found that there are significant points of resemblance between the phenomenology of the noncentrally fueled sandpile and of the tokamaks with off-axis ECH. This suggests that the essential ingredient of the sandpile model, namely avalanching conditioned by a local critical gradient, may be one of the key transport effects generated by the tokamak plasma physics. © *2004 American Institute of Physics.* [DOI: 10.1063/1.1639017]

I. INTRODUCTION

Electron cyclotron heating (ECH) provides a means for delivering energy to a region of a tokamak plasma that is highly localized in the radial spatial coordinate. This localization follows from the nature of the cyclotron resonant condition between the incident wave and the electrons, including Doppler and relativistic effects.[1–3] Rapid transport of heat along magnetic field lines ensures that, initially, ECH energy is swiftly and evenly spread toroidally and poloidally over the family of magnetic surfaces on which it was first deposited, whose radial extent is relatively narrow. On longer time scales, radial transport of this energy across the plasma is governed by: (1) the physics of electron energy transport perpendicular to the applied magnetic field, which includes turbulent as well as diffusive processes; and (2) the radial temperature profile, to which energy deposited through ECH both responds and contributes. For these reasons, observations of the response of tokamak plasmas to ECH can provide a fundamental probe of the underlying physics of transport and confinement, particularly when advantage is taken of the capability to localize ECH spatially and temporally. Several such observations provide evidence that simple diffusive transport models are not sufficient in isolation to interpret all the data; for a review see Ref. 4. In parallel, studies[5–17] of avalanching transport, self-organization, and non-Gaussian statistics in tokamak plasma turbulence, have played a key role in the addition of nonlocal transport paradigms, notably the sandpile,[18,19] to the repertoire of fusion plasma confinement physics. An attraction of the sandpile approach to modeling nondiffusive transport is that the behavior that emerges is independent of the detailed choice of sandpile algorithm, except insofar as a particular control parameter (such as our L_f, described below) is deliberately introduced. If a simple sandpile model reproduces key aspects of the behavior of a real system, this may also assist the interpretation of more complex models that have more detailed physical motivation.

In the present paper, we focus on the possible implications of certain phenomena observed in classic off-axis ECH experiments reported on the DIII-D[20,21] and Rijnhuizen Tokamak Project (RTP)[22,23] tokamaks, which we outline below. As noted by the experimenters, it is clear that these experiments contain information on the balance between diffusive and nondiffusive (for example, avalanching) transport processes in determining the observed phenomenology. One way of extracting some of this information is to investigate how far the sandpile paradigm can capture key aspects of the plasma behavior which is observed. This applies particularly to features of the observed plasma behavior that are strongly nonlinear, and therefore difficult to capture using the conventional analytical techniques of plasma physics. In this paper,

we report progress on this question, which has required the development and application of a sandpile model that incorporates off-axis fueling. Our starting point is the particular sandpile model described in Ref. 24, whose relevance to tokamak phenomenology is well established;[13,17] the adaptations necessary to incorporate noncentral fueling are described in Sec. II. In Secs. III and IV we compare outputs of our sandpile model with specific aspects of observed plasma behavior in the DIII-D and RTP tokamaks, respectively. Sandpile models are, of course, much simpler systems than tokamak plasmas and can, therefore, display only a subset of the phenomenology seen in tokamaks. Insofar as the output from our sandpile model resembles aspects of the observations of transport phenomena associated with off-axis ECH in tokamaks, we hypothesize that the essential ingredient of the algorithm (avalanching transport conditioned by a local critical gradient) may be one of the key transport effects generated by the underlying plasma physics.

II. SANDPILE MODEL INCORPORATING OFF-AXIS FUELING

The sandpile algorithm operates on a one-dimensional (1D) grid of N cells each containing a real valued height of sand, the height in the kth cell being denoted h_k. Cell $k = 1$ corresponds to the core (axis of symmetry) of the plasma, and cell $k = N$ corresponds to the plasma boundary. Thus k/N corresponds to the dimensionless variable $\rho = r/a$, where r is the minor radial coordinate and a is the minor radius of the plasma boundary, so that $0 < \rho \leq 1$. The height of sand is taken to be a proxy for the plasma quantity of interest, which as we shall see is electron thermal energy in the present case. Thus the profile of the 1D sandpile is intended to model features of the 1D electron temperature profile of a tokamak across its minor radius.

Transport in the sandpile model is through avalanches, and this is achieved as follows. A cell k is said to be critical if

$$h_k - h_{k\pm1} > z_{c_k}, \tag{1}$$

that is when the local gradient of the sandpile exceeds a defined local *critical gradient* z_{c_k}. If a cell is critical then sand is redistributed to neighboring cells, which may in consequence turn critical, leading to further redistribution—in short, an avalanche—which continues until the sandpile is everywhere subcritical. The avalanching process is instantaneous insofar as there is no further fueling while an avalanche progresses. Sand is locally redistributed around the critical cell such that the region nearby is left at the *repose gradient* z_r. In our model, redistribution involves a flattening-back region extending forwards (downhill) one cell from the critical cell, and backwards (uphill) P cells. Here P is a variable length parameter which is determined anew, internally by the sandpile algorithm, each time the critical gradient is exceeded. In the original model of Ref. 24, the parameter P is the maximum distance allowed either by the proximity of the system boundary or a maximum value L_f, the fluidization length parameter. In the new model, in order to allow off-axis fueling, an additional limit
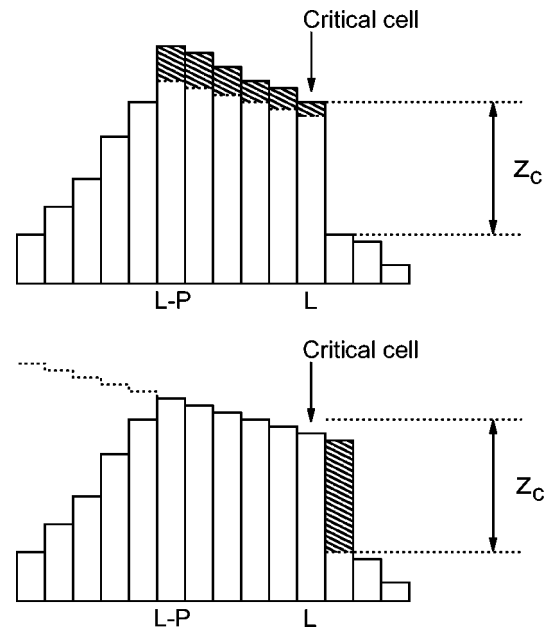

FIG. 1. Section of sandpile prior to flattening (top) and after flattening (bottom). Cells involved in flattening are numbered $L - P$ to $L + 1$ with the critical cell numbered cell L. Sand is redistributed from cells $L - P$ to L onto cell $L + 1$. Flattening does not continue beyond a backward distance P. The dotted line shows the repose gradient: If flattening continued further back it would result in an increase in height of the rearmost cells.

is imposed on P to prevent upward transport of sand. If P is too large (extending back beyond the fueling location) a redistribution of sand could lead to an increase in the height of the rearmost cells in the fluidization region (see Fig. 1). The precise condition on P is explained in the Appendix. The effect of the parameter L_f on the model is explained fully in Ref. 24.

To simulate off-axis deposition, the sandpile is driven by the continuous addition of single grains of sand to a designated cell f

$$h_f \rightarrow h_f' = h_f + 1. \tag{2}$$

This defines a fueling radius R_S

$$R_S = f/N. \tag{3}$$

Sand must be able to flow in either direction, left or right. Mathematically, this is implemented in the sandpile algorithm by referring simply to forward and backward directions relative to the local slope. Suppose that cell k, which may be anywhere in the sandpile, has become critical. For redistribution algorithm purposes, we set up a local renumbering of the cells, fixed about the critical cell k which we now label cell L. Sand is distributed from uphill cells extending back up the pile to cell $L - P$; this sand is moved downhill to cell $L + 1$. A detailed description of the algorithm for determining P and redistributing sand is provided in the Appendix. The original sandpile algorithm of Ref. 24, modified to accommodate noncentral fueling by incorporating a variable fluidization length, which changes as described for each iteration, allows sand to flow in either direction with respect to R_S.
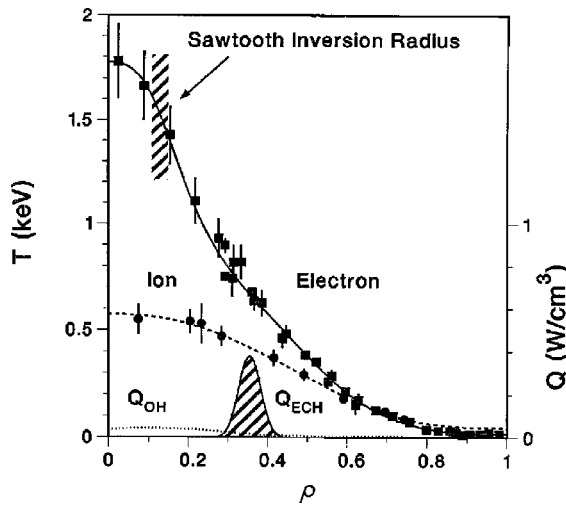
FIG. 2. Plasma profiles for a DIII-D L mode discharge with off-axis ECH. Electron and ion temperature profiles; the first pass ECH and ohmic heating profiles are also shown. Reproduced from Ref. 21.

FIG. 4. Increase in the average height profile above the reposed pile at different times after switch-on of off-axis fueling. Each profile is an average over 2×10^5 sequential additions of sand grains, beginning at fueling event times as follows: Dash–dot line, 8×10^5 grains; dashed line, 10×10^5 grains; solid line, 12×10^5 grains. The sandpile is fueled at cell 200 with $z_c = 100$ grains, and the control parameter (see the Appendix) $L_f = 400$.

III. RELATION TO TIME EVOLUTION OF RADIAL TEMPERATURE PROFILES IN DIII-D

One instance of the observational motivation for our approach is provided by Fig. 4 of Ref. 21, reproduced here as Fig. 2. This shows a centrally peaked radial profile for electron temperature T_e obtained for an L-mode discharge in DIII-D subjected to off-axis ECH around $R_S = r/a = 0.35$. As noted by the original authors, it is evident that there must be inward nondiffusive transport that can be uphill with respect to the radial gradient dT_e/dr, and this is confirmed by rigorous analysis.[21] These conclusions are supplemented by Fig. 8 of Ref. 21, shown here as Fig. 3, which shows radial profiles of the enhancement of T_e during ECH at four different times spanning 200 ms. At the earliest time after onset of ECH, the enhancement of T_e is spatially localized about the
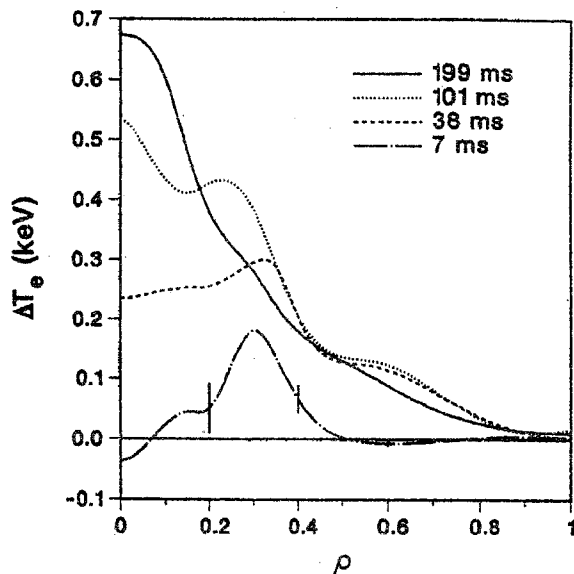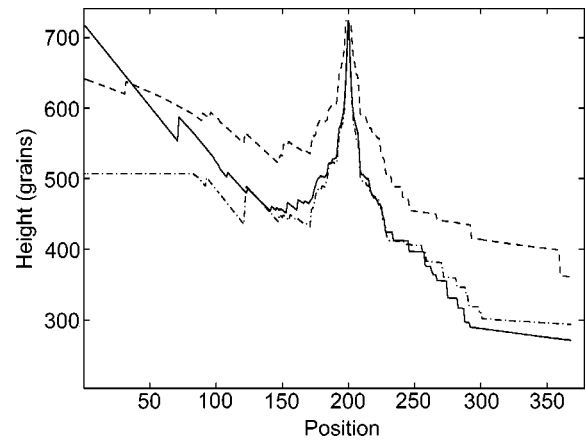

FIG. 3. Increase in the electron temperature above the ohmic value at four different times after the start of ECH for the DIII-D discharge shown in Fig. 2. Reproduced from Ref. 21.

ECH deposition region, where it peaks, whereas its magnitude is small for $r/a \simeq 0$ and $r/a \simeq 1$. At the next snapshot, the T_e enhancement outboard of the deposition region ($r/a > R_S$) corresponds roughly to the final profile achieved, with dT_e/dr negative; inboard ($r/a < R_S$), there is now significant enhancement, with dT_e/dr positive. The final two snapshots show invariant outboard profiles, while there is steady infill inboard, where dT_e/dr shifts from positive to negative. A vestigial local peak at the deposition region only disappears in the final snapshot, where a situation corresponding to Fig. 2 is recovered.

We now turn to relevant results obtained from the sandpile model described in Sec. II. Figure 4 shows three traces which display the time evolution of the enhancement of the height profile of the sandpile above its fully reposed state, with off-axis fueling. The profiles are time-averaged, in that they are calculated by taking the mean of 2×10^5 sequential profiles, corresponding to 2×10^5 sequential fueling events (additions of single grains of sand). The earlier trace (dash–dot line) shows the time-averaged profile beginning at fueling event number 8×10^5. The latter traces (dashed line and solid line) show the time-averaged profiles over the subsequent 2×10^5 grain intervals. In this instance of the model L_f is set at 400 cells and z_c is 100 grains. Comparison of the traces shows two features that are common to the tokamak observations shown in Fig. 3. First, there is infill inboard of the fueling location ($r/a < R_S$), leading to a centrally peaked profile. This has arisen from nondiffusive avalanching transport that is able to operate uphill with respect to the mean local gradient [compare with the previous discussion of Fig. 2 (Fig. 4 of Ref. 21)]. Second, and in contrast, the slope outboard of the fueling location ($r/a > R_S$) does not change significantly. This is because in the outboard region, the sandpile has already risen to the typical average slope that is compatible with the critical gradient and the processes of fueling and loss. The temporally intermediate (dashed) trace in Fig. 4 illustrates two features of sandpile transport that give rise to the profile evolution that is seen. Inboard of the

fueling point there are steep local reverse gradients that give rise to avalanching transport of sand that is uphill with respect to the mean overall gradient. Outboard of the fueling point there is an excess of sand over the final state, while the mean gradient is lower than in the final state; this excess is subsequently lost through outward-propagating avalanches, as fueling continues and the mean gradient steepens. A point of difference with the tokamak observations is the local peak at the fueling position. This persists in the sandpile model, but disappears as the tokamak profile evolves in time. The reason for this difference is that transport in the sandpile model contains no diffusive component, whereas a diffusive component to the plasma transport would (and presumably does) eliminate this local structure in the tokamak.

We conclude that avalanching transport combined with off-axis fueling may indeed be responsible for key aspects of the otherwise paradoxical tokamak observations discussed in this section. It is seldom possible to determine experimentally the relative weighting of avalanching and diffusive components of the plasma transport at any particular locale in any particular tokamak discharge. The DIII-D observations point to a substantial, and in some regions dominant, avalanching component in the plasmas considered.

IV. RELATION TO RADIAL TEMPERATURE AND DENSITY PROFILES IN RTP

A second set of applications for our sandpile model is provided by observations of electron energy transport in the RTP tokamak. Here there is strong observational evidence for the existence of multiple narrow localized transport barriers. For example, Fig. 7 of Ref. 23, which plots central electron temperature against the radial location of off-axis ECH energy deposition, exhibits a sequence of sharp plateaux. This is a dramatic instance of self-organization in a macroscopic plasma, and its origin is the subject of intense research. It seems likely that the magnetic field plays a central role in the location and formation of these transport barriers, while numerical simulations (for example, Ref. 25) of the plasma turbulent transport in RTP suggest that avalanching transport may also play a role. There remains an important supplementary question: What forms of electron energy transport are compatible with the observed shape and time evolution of the radial temperature profiles? In particular, do these observations suggest that the plasma transport processes include an avalanching component? The sandpile model outlined in Sec. II does not assume the existence of internal transport barriers. Nevertheless, as we shall see, the model's incorporation of avalanching transport coupled to off-axis fueling is sufficient to give rise to phenomenology resembling aspects of that observed in RTP. Specifically, in this section we consider two sets of observations. In Sec. IV A, we consider observations of radial electron temperature profiles that are hollow and have "ears" near the energy deposition location, shown in Figs. 8, 16, and 17 of Ref. 23. The temperature profile outboard of the deposition point is relatively invariant. In Sec. IV B, we consider observed correlations in the temporal evolution of electron temperature measured simultaneously at the plasma center and at the off-
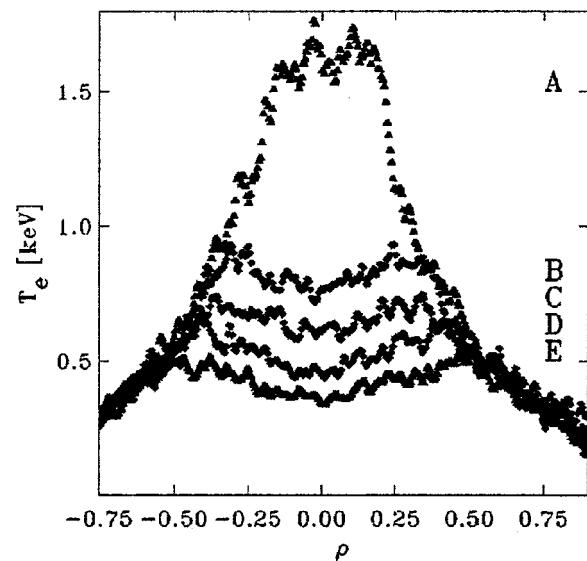

FIG. 5. Examples of electron temperature profiles for discharges in RTP. Note that the outer part of the profiles almost coincide. Reproduced from Ref. 23.

axis energy deposition location. We refer in particular to measurements during time intervals that incorporate major crashes in central electron temperature, see Figs. 6 and 7 of Ref. 22.

A. Hollow temperature profiles with "ears"

Figures 5 and 6 (Figs. 8 and 17 of Ref. 23), show electron temperature profiles obtained in the RTP tokamak for different locations of off-axis ECH energy deposition. The extremely high resolution of the Thomson scattering techniques used in RTP yields two major benefits. First, the number of data points in the spatial profiles is very high. Second, the location of the peak ECH energy deposition point with respect to the measured sequence of radial transport barriers is well determined. Figure 5 shows that as the off-axis deposition location is moved outwards, correspondingly broader hollow electron temperature profiles result. In parallel, the peak central temperature falls, while the outboard gradient ($r/a > R_S$) is almost invariant. Figure 6 shows that when ECH is deposited just inboard of a transport barrier (r/a
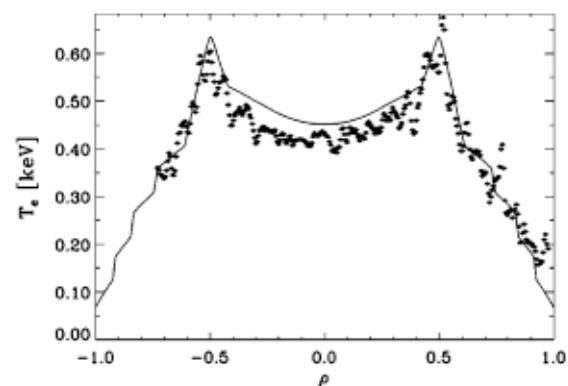

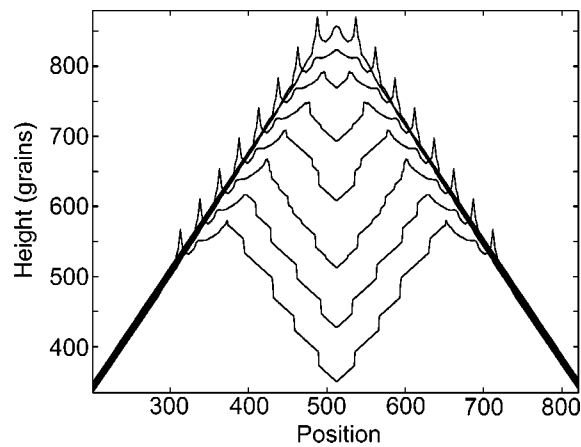FIG. 6. RTP electron temperature profile displaying conspicuous "ears." Reproduced from Ref. 23.

FIG. 7. Examples of average height profiles over 10^9 sand grains for multiple runs of the sandpile model with different off-axis fueling positions at cell locations 25, 50,...,200. Mirror symmetry is imposed. The critical gradient $z_c = 10$; the control parameter (see the Appendix) $L_f = 50$.
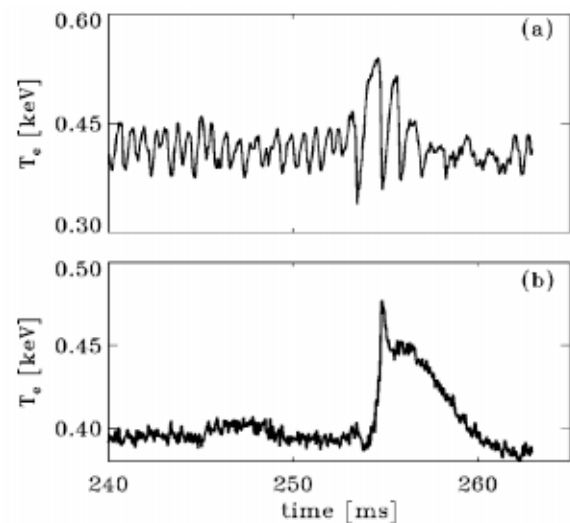

FIG. 8. Time series of RTP electron temperature at the fueling position (a) and in the center (b) showing minor crashes and one major crash. Reproduced from Ref. 22.

$\langle R_S \rangle$), well defined ears appear in the electron temperature profile near the deposition point. We now use our sandpile model to investigate whether these observations are consistent with the suggestion that the plasma transport incorporates a nondiffusive component, such as avalanching.

Figure 7 shows sets of steady-state average sandpile height profiles averaged over 10^9 sand grains, for different off-axis fueling locations with $z_c = 10$ and $L_f = 50$. For purposes of comparison with the tokamak profiles noted above, which extend across the plasma from the inner to the outer boundaries, Fig. 7 shows sandpile profiles obtained by mirroring the final data about the pile center. The center of the sandpile is labeled cell number $n = 1$, and separate profiles are obtained for off-axis fueling locations at cells 25, 50,..., 200. There are four points of contact between the form of the sandpile profiles in Fig. 7, and the RTP results shown in Figs. 5 and 6. First, we have mostly hollow profiles whose central height falls as the fueling location is moved further off-axis. Second, for fueling locations that are not far off-axis, the inboard portion of the profile is approximately flat. Third, the outboard profile is independent of fueling location. Fourth, there are ears resembling those in Fig. 6. The fact that these features arise naturally from a very simple sandpile model suggests that avalanching transport may play a significant role among the various plasma physics processes that together determine the RTP profiles considered.

The profiles in Fig. 7 shed light on the mechanism for inward transport evident in Fig. 4. When the critical gradient is exceeded at a point, this triggers redistribution over a distance that extends backwards over a distance P, as previously described. Potentially, this may extend back past the fueling position, a contingency that did not require consideration in the original model of Ref. 24. As the sandpile evolves, this class of redistribution event gives rise to a small region, inboard of the fueling location, whose slope has the same sign as that in the outboard region. This inboard ramp region is visible in Fig. 7, adjacent to the fueling location ears. The ramp region permits sustained central concavity, by blocking the progress of inboard-traveling avalanches, except when

the fueling location is close to the center of the sandpile. In the latter case, the ramp regions coalesce, resulting in a filled profile such as that shown in Fig. 4. The extent of the ramp region is determined by the fluidization parameter L_f.

B. Correlated behavior during central electron temperature crashes

We now consider Fig. 6 of Ref. 22, shown here as Fig. 8. This shows two points of particular interest to us. First, in the run-up to a major crash in central electron temperature in RTP, the amplitude of temperature fluctuations is greater at the ECH deposition point than at the center. Second, the major crash has a more sharply defined leading edge at the center; thereafter it relaxes almost monotonically, whereas the temperature at the deposition point oscillates several times during this interval. Figure 9 shows that similar behavior occurs naturally in our sandpile model. The upper trace of
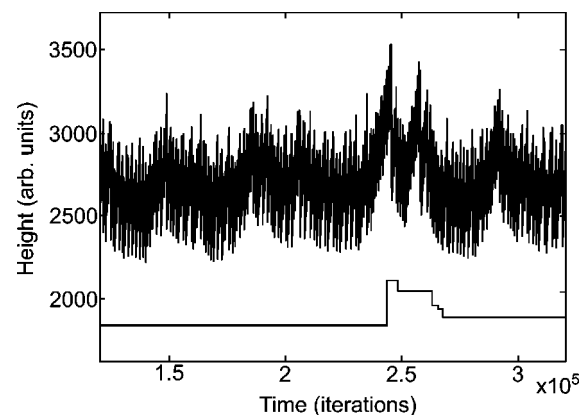

FIG. 9. Time series of sandpile height at the fueling position (upper) and in the center (lower), showing a number of minor crashes and a single major crash. The horizontal (time) axis is measured in number of sand grains added; critical gradient $z_c = 100$, control parameter (see the Appendix) $L_f = 200$.
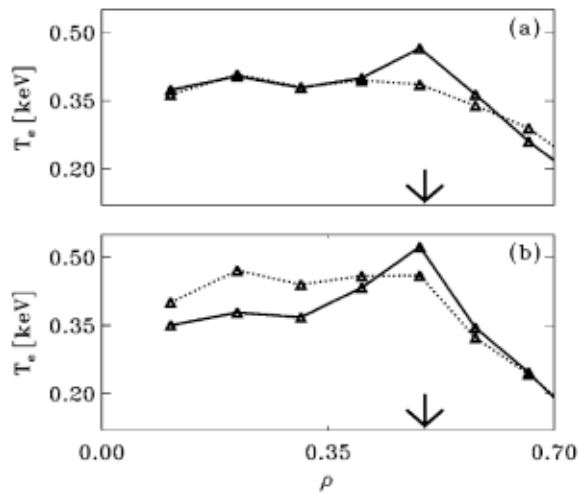
FIG. 10. Electron temperature profile in RTP just before (solid line) and after (dotted line) a minor crash (a) and a major crash (b). The minor crash affects only the region near the fueling position, whereas the major crash affects the whole central plasma. Reproduced from Ref. 22.

Fig. 9 (which like Fig. 7 is mirrored) shows the time evolution of the height of the sandpile at its central cell ($n=1$ here), while the lower trace shows the simultaneous time evolution of the height of the sandpile at its off-axis fueling point ($n=100$). Turning to Fig. 7 of Ref. 22, Fig. 10 here, we see that before a major crash, the radial electron temperature profile at the deposition point is locally peaked: Inboard, it declines locally to form the hollow profile; outboard, it declines steadily towards the plasma edge. After a major crash, there is no local peak: The temperature profile inboard is flat; outboard, the gradient is similar to before the crash. Figure 11 shows that somewhat similar behavior occurs naturally in our sandpile model. Comparison of sandpile profiles taken immediately before and after a major central crash shows that the crash results in inboard rise and flattening, a greatly diminished local peak, and outboard invariance. Again, it appears reasonable to infer that avalanching transport may be playing a significant role in generating the observed tokamak phenomenology.
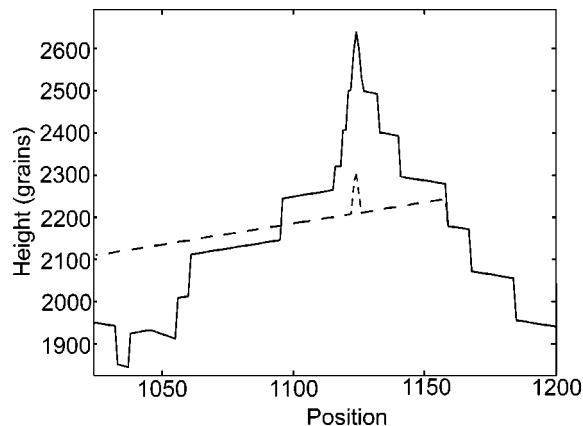

FIG. 11. Average height profiles showing pile configuration just before (solid line) and after (dotted line) the major crash event shown in Fig. 9.

C. Sand: A proxy for plasma density or electron thermal energy?

These results also shed light on the general question whether sand, as transported by sandpile models, corresponds more closely to plasma density or to plasma thermal energy. Measurements on RTP show that plasma electron temperature exhibits hollow profiles under off-axis ECH, whereas plasma density does not. Indeed transitions to lower temperature plateaux correspond to increasingly centrally peaked density profiles, see in particular Fig. 9 of Ref. 23. We conclude that, insofar as the profiles generated by our sandpile algorithm are hollow rather than peaked under off-axis fueling, the sand corresponds to thermal energy and not plasma density.

We note that the inward transport of sand in the model does not violate any fundamental physical principle. All avalanches dissipate energy and sand always moves downhill from the point at which it was first injected. The growth of sandpile height inboard of the fueling point results from sand grains moving downhill from transient local peaks around the fueling position. These are not seen in the average height profiles but can be observed in instantaneous snapshots.

V. CONCLUSIONS

We have used a specific sandpile model to generate steady-state profiles and related time-varying phenomenology that have significant points of contact with the corresponding observed consequences of off-axis ECH in the DIII-D and RTP tokamaks. As noted by the original observers, many of the tokamak effects are paradoxical when viewed from the perspective of a diffusive transport paradigm. It is clear that they constitute important items of evidence bearing on the general question of the balance between diffusive and nondiffusive (for example, avalanching) transport in different tokamak plasmas. Direct observation of electron transport processes during ECH is problematic (see, for example, the discussion in Ref. 12), however, it is possible to draw inferences about these processes from the combination of profile observations and transport modeling, as here. The results of the present paper support the hypothesis that avalanching transport may play a role in many plasmas, and that in some circumstances it can provide a mechanism for the dominant observed effects.

APPENDIX: DETAILS OF REDISTRIBUTION IN THE SANDPILE ALGORITHM

The total mass of sand in the flattening-back region is given by

$$S = \sum_{i=L-P}^{L+1} h_i. \tag{A1}$$

After flattening, the height of a cell in the region is given by

$$h_i' = h_{L-P}' - (i-1)z_r, \tag{A2}$$

where

$$h_{L-P}' = \frac{S}{P+2} + \frac{(P+2)z_r}{2}, \tag{A3}$$

gives the height of the trailing edge at cell $L-P$ after flattening. The term on the left is simply the mean height of sand in the region and this corresponds to the height of the central cell after flattening. The term on the right is the extra height introduced by half the width of the region at a slope of z_r.

The magnitude of P determines how much of the sandpile is affected by any single flattening event. In the original algorithm of Ref. 24, where sand is added adjacent to a closed boundary, this is limited by a maximum value L_f, the *fluidization length*, and by the system boundary. Here we must impose an additional limit on P. The flattening-back region must not extend back uphill to cells where the subsequent redistribution of sand would cause their height to increase. This would correspond to an unphysical situation of sand propagating uphill. The region is, therefore, limited to the last cell where redistribution would cause a height decrease. Graphically this approximately corresponds to the point where a reposed pile would intersect the unreposed pile, see Fig. 1. The algorithm operates by considering first a flattening-back region with $P=0$. The length of the region is gradually increased while keeping track of the total mass of sand enclosed. For every increasing P, the flattened height of the first uphill cell in the region h_{L-P}' is evaluated from Eq. (A3) and compared with its actual value h_{L-P}. This process continues until either

$$h_{L-P}' > h_{L-P} \quad \text{from Eq. (A3)}, \tag{A4}$$

$$\text{OR} \quad P = L_f - 1, \tag{A5}$$

OR cell $L-P$ coincides with a boundary. $\quad$ (A6)

This establishes a value for P consistent with the fluidization length parameter L_f, the system boundary, and the requirement that sand grains flow only downhill.

[1] M. Bornatici, R. Cano, O. de Barbieri, and F. Engelmann, Nucl. Fusion **23**, 1153 (1983).
[2] B. Lloyd, Plasma Phys. Controlled Fusion **40**, A119 (1998).
[3] T. C. Luce, IEEE Trans. Plasma Sci. **30**, 734 (2002).
[4] J. D. Callen and M. W. Kissick, Plasma Phys. Controlled Fusion **39**, B173 (1997).
[5] D. E. Newman, B. A. Carreras, P. H. Diamond, and T. S. Hahm, Phys. Plasmas **3**, 1858 (1996).
[6] B. A. Carreras, D. Newman, V. E. Lynch, and P. H. Diamond, Phys. Plasmas **3**, 2903 (1996).
[7] R. O. Dendy and P. Helander, Plasma Phys. Controlled Fusion **39**, 1947 (1997).
[8] B. A. Carreras, B. van Milligan, M. A. Pedrosa *et al.*, Phys. Rev. Lett. **80**, 4438 (1998).
[9] M. A. Pedrosa, C. Hidalgo, B. A. Carreras *et al.*, Phys. Rev. Lett. **82**, 3621 (1999).
[10] S. C. Chapman, R. O. Dendy, and G. Rowlands, Phys. Plasmas **6**, 4169 (1999).
[11] T. L. Rhodes, R. A. Moyer, R. Groebner, E. J. Doyle, R. Lehmer, W. A. Peebles, and C. L. Rettig, Phys. Lett. A **253**, 181 (1999).
[12] P. A. Politzer, Phys. Rev. Lett. **84**, 1192 (2000).
[13] S. C. Chapman, R. O. Dendy, and B. Hnat, Phys. Rev. Lett. **86**, 2814 (2001).
[14] H. R. Hicks and B. A. Carreras, Phys. Plasmas **8**, 3277 (2001).
[15] J. P. Graves, R. O. Dendy, K. I. Hopcraft, and E. Jakeman, Phys. Plasmas **9**, 1596 (2002).
[16] I. Gruzinov, P. H. Diamond, and M. N. Rosenbluth, Phys. Rev. Lett. **89**, 255001 (2003).
[17] S. C. Chapman, R. O. Dendy, and B. Hnat, Plasma Phys. Controlled Fusion **45**, 301 (2003).
[18] P. Bak, C. Tang, and K. Wiesenfeld, Phys. Rev. Lett. **59**, 381 (1987).
[19] P. Bak, C. Tang, and K. Wiesenfeld, Phys. Rev. A **38**, 364 (1988).
[20] T. C. Luce, C. C. Petty, and J. C. M. de Haas, Phys. Rev. Lett. **68**, 52 (1992).
[21] C. C. Petty and T. C. Luce, Nucl. Fusion **34**, 121 (1994).
[22] M. R. de Baar, G. M. D. Hogeweij, N. J. Lopes Cardozo, A. A. M. Oomens, and F. C. Schüller, Phys. Rev. Lett. **78**, 4573 (1997).
[23] M. R. de Baar, M. N. A. Beurskens, G. M. D. Hogeweij, and N. J. Lopes Cardozo, Phys. Plasmas **6**, 4645 (1999).
[24] S. C. Chapman, Phys. Rev. E **62**, 1905 (2000).
[25] A. Thyagaraja, Plasma Phys. Controlled Fusion **42**, B255 (2000).